Using reduced data sets ISCCP-B2 from the Meteosat satellites to assess surface solar irradiance

Mireille Lefèvre, Lucien Wald, Lamissa Diabate

Lefèvre M., Diabaté L., Wald L., Using reduced data sets ISCCP-B2 from the Meteosat satellites to assess surface surface solar irradiance. Solar Energy, 81, 240-253, 2007, doi:10.1016/j.solener.2006.03.008.

USING REDUCED DATA SETS ISCCP-B2 FROM THE METEOSAT SATELLITES TO ASSESS SURFACE SOLAR IRRADIANCE

M. Lefèvre (1), L. Wald (1), L. Diabaté (2)

(1) Centre Energétique et Procédés, Ecole des Mines de Paris / Armines, BP 207, 06904, Sophia Antipolis cedex, France

(2) UFAE / GCMI, BP E4018, 410, avenue Van Vollenhoven, Bamako, Mali

Corresponding author: Lucien Wald, lucien.wald@ensmp.fr

ABSTRACT

This paper explores the capabilities of a combination of the reduced data set ISCCP-B2 from the Meteosat satellites and the recently developed method Heliosat-2 to assess the daily mean of the surface solar irradiance at any geographical site in Europe and Africa. Firstly, we discuss the implementation of the method Heliosat-2. Secondly, B2-derived irradiances are compared to coincident measurements made in meteorological networks for 90 stations from 1994 to 1997. Bias is less than 1 W m^{-2} for the whole set. Larger bias may be observed at individual sites, ranging from -15 to +32 W m^{-2}. For the whole set, the root mean square difference is 35 W m^{-2} (17%) for daily mean irradiance and 25 W m^{-2} (12%) for monthly mean irradiance. These accuracies are close to those of similar data sets of irradiance, such as Medias and NASA Surface Radiation Budget. It is concluded that B2 data can be used in a reliable way to produce long-term time-series of irradiance for Europe, Africa and the Atlantic Ocean.

Keywords: Satellite, radiation, fluxes, climatology, Africa, Europe, Atlantic Ocean

1. NOMENCLATURE

t	time.
θ_S	sun zenithal angle for the pixel under concern (radian)
θ_S^{noon}	sun zenithal angle at noon for the pixel under concern (radian)
θ_V	satellite viewing angle, formed by the normal to the ground and the direction of the satellite for the pixel under concern. It is the complement to 90° of the satellite altitude angle above horizon (radian)
TL	Linke turbidity factor for a relative air mass equal to 2 (unitless)
I	irradiance observed at ground level on horizontal plane, called SSI (surface solar irradiance) (W m^{-2})
I_d	as I but averaged over one day (W m^{-2})
I_c	SSI under very clear skies (W m^{-2})
I_{cd}	as I_c but averaged over one day (W m^{-2})
K_c	clear-sky index. It is equal to the ratio of I to I_c (unitless)
KT	clearness index. It is equal to the ratio of I to the irradiance observed outside the atmosphere (unitless)
ρ^t	reflectance observed by the spaceborne sensor at instant t (unitless)
$\rho_\alpha{}^t$	apparent reflectance of the ground at instant t (unitless)
ρ_{eff}	effective reflectance of the brightest clouds (unitless)
ρ_{cloud}	apparent cloud albedo observed by the spaceborne sensor over the brightest clouds (unitless). It is a quantity specific to the method Heliosat
ρ_g	ground reflectance (unitless)
ρ_g^{ref}	reference ground reflectance (unitless)
ρ_{atm}	intrinsic reflectance of the clear atmosphere (unitless)
T	transmittance of the clear atmosphere (unitless)
n	cloud index (unitless)
Φ_P, Φ_X	latitude of respectively a point $\boldsymbol{P}$, a point $\boldsymbol{X}$ (decimal degrees)
d_{geo}	geodetic distance (km)
d_{eff}	effective distance (km)

f_{NS} a unitless parameter for interpolation taking into account the latitudinal asymmetry of the climate phenomena

δh difference in elevation between the point ***P*** and another site ***X*** (km)

f_{oro} a unitless parameter for interpolation taking into account the difference in elevation (=500)

2. INTRODUCTION

This paper deals with the assessment of the irradiance observed at ground level on horizontal surfaces, also called surface solar irradiance (SSI). Accurate assessments can now be drawn from satellite data, especially from the geostationary meteorological satellites such as Meteosat covering Europe and Africa. Several studies demonstrate the superiority of the use of satellite data over interpolation methods applied to measurements performed within a radiometric network (Perez et al., 1997; Zelenka et al., 1992, 1999). Based on satellite data, the project Surface Radiation Budget (SRB) is offering accurate monthly means of SSI for several years and the whole Earth with a low spatial resolution (Whitlock et al., 1995; Darnell et al., 1996). However, there is a demand for more detailed information in space and time with an emphasis for long-term time-series of irradiance. Several atlases, digital or not, were produced offering spatial resolutions better than 1° of arc angle: Raschke et al. (1991), Medias (1996) and ESRA (2000). Several national weather bureaus are currently using satellite data to map the SSI, e.g., Hungary (Rimoczi-Paal et al*.,* 1999) or Australia (AGSRA, 2003). These initiatives do not fully answer the demand because they cover a limited area or a limited period.

One obstacle to the production of such information is the large amount of data to process. Take the example of the satellite system within the Meteosat Operational Programme (MOP). One third of the Earth is imaged every 0.5 h in a broadband range (0.4 – 1.1 micron) with a pixel size of 2.5 km at nadir. This creates an image of 5000 x 5000 pixels. A data set of reduced spatial resolution, called ISCCP-B2 data, was created for the International Satellite Cloud Climatology Project (ISCCP) to better handle and exploit this wealth of information (Schiffer and Rossow, 1985). If one keeps only the pixels that can be processed to produce SSI, i.e., approximately 70% of the whole image, one year of data means approximately a volume of 243 Gigabytes for high-resolution data and 0.2 only for B2 data. Using B2 data permits very large gains in data storage, especially when contemplating the creation of an archive of 20 years or more as we do. In addition, B2 data were cheaper than high-resolution

data, at least for Meteosat satellites and before the latest changes in data policy of Eumetsat, the owner of the Meteosat data. For example, ten years ago, when our project started, one year of high-resolution data was more than 20 keuro worth while the cost was only 500 euro for B2 data. This was the second reason for choosing B2 data. Figure 1 displays an example of a B2 image for Meteosat.

Several authors already used B2 data for the assessment of the SSI (Ba et al., 2001; Raschke et al., 1987; Tuzet et al., 1984). These works clearly demonstrated the interest of B2 data for producing long-term time-series of SSI over large periods. However, the assessment of the quality of the B2-derived SSI is limited in these papers in the number of sites and period of time. This paper addresses this problem. It explores the capabilities of a combination of the B2 data set and the recently developed method Heliosat-2 to assess the SSI at any geographical site in Europe and Africa. In addition, it describes the operational implementation of the method Heliosat-2. This implementation was performed by using the software libraries that are freely available at the web site www.helioclim.net.

3. THE METHOD HELIOSAT-2 AND ITS IMPLEMENTATION

The model for converting satellite data into SSI is the method Heliosat-2 proposed by Rigollier et al. (2004, abbreviated RLW in the following). This method is particularly suitable for processing time-series of data acquired by a series of sensors that are similar but differ slightly in calibration as it is the case of the Meteosat system prior to 1998 (Anonymous 1996). It is based on the principle that the attenuation of the downwelling shortwave radiation by the atmosphere over a pixel is determined by the magnitude of change between the reflectance that should be observed under a very clear sky and that currently observed (Pastre, 1981; Cano et al., 1986; Stuhlmann et al., 1990). In the method Heliosat-2, the SSI is computed by the means of the clear-sky index K_c defined as:

$$K_c = I / I_c \qquad (1)$$

where I_c is the SSI under clear skies. The clear-sky index K_c is derived from the satellite images as explained later. I_c is modelled by a clear-sky model. Two other quantities are instrumental in this method: the reflectance of the ground (also called the ground albedo) and that of very reflective clouds.

3.1 The clear-sky model

The clear-sky model provides I_c. RLW discuss the choice of the ESRA model (Rigollier et al., 2000). The inputs to this model are the solar zenithal angle θ_S, the elevation of the site and the Linke turbidity factor for a relative air mass 2, *TL*. The database TerrainBase (1995) is adopted for elevation; it contains the mean elevation for each cell of 5' of arc angle worldwide. The Linke turbidity factor *TL* is a very convenient approximation to model the atmospheric absorption and scattering of the solar radiation under clear skies. It describes the optical thickness of the atmosphere due to both the absorption by the water vapour and the absorption and scattering by the aerosols relative to a dry and clean atmosphere. Like the water vapour and the aerosol optical parameters, *TL* is known at a limited number of sites. It greatly varies in space and in time. Remund et al. (2003) collected a number of observed values of *TL* worldwide and merged these values with gridded maps of *TL* derived from the ISCCP clear-sky SSI at coarse resolution (approx. 300 km), other maps of water vapour and aerosol optical properties and the database TerrainBase. The fusion of these various sets of data created a series of 12 maps, one per month, covering the world with a cell of 5' (approximately 10 km at mid-latitude).

This database of *TL* is available from Les Presses, Ecole des Mines de Paris, and we use it as an input. There is one value per month; time interpolation is performed for each day. As these are typical values of *TL* for a month, the discrepancies between the database and the actual values lead to errors in assessing the SSI as indicated by Eq. 1. *TL* may vary greatly from one hour to another, or one day to another. It is often set to 3.5 in Europe as an average but large variations may be observed from 2.5 to 5 typically in urban areas with heavy vehicle traffic between early morning when there is no pollution and the afternoon with pollution at its maximum. According to graphs in Rigollier et al. (2000), a change of 1 in *TL* leads to a relative change of approximately 10 – 15% in I_c and thus in *I*. The sensitivity of the outcomes of the method Heliosat-2 to *TL* is studied by RLW by the means of a comparison with one year of ground measurements made at 35 sites in Europe. By setting *TL* to typical values for each site and then to a fixed value of 3.5, RLW found that the bias between measured SSI and Heliosat-2-derived SSI is sensitive to the selected values of *TL*. The largest discrepancies are found when the sun is low above the horizon. RLW note that the influence is not limited to clear-sky cases. Besides this source of error, we should mention that the database exhibits exaggerated spatial gradients that were created artificially by the fusion process. These gradients will appear in the resulting SSI maps (Eq. 1) and this is another source of error. Nevertheless, this database is the only source we know of *TL* for every pixel of the Meteosat images and this is a good reason to use it.

Using this ESRA model, RLW compute the intrinsic reflectance of the atmosphere, ρ_{atm}, the downward (sun to ground) and upward (ground to satellite) transmittances of the clear atmosphere $T(\theta_S)$ and $T(\theta_V)$, where θ_V is the satellite viewing angle, formed by the normal to the ground and the direction of the satellite. By comparison with radiative transfer models and ground measurements, RLW find that the accuracy in the retrieval of these quantities degrades for θ_S or θ_v greater than 75°. They recommend to not using the method Heliosat-2 for such angles.

3.2 The reflectance of the ground

Under clear skies, the actual reflectance of the ground, ρ_g, is approximately equal to:

$$\rho_g = [\rho^t - \rho_{atm}] / T(\theta_S)\, T(\theta_v) \qquad (2)$$

where ρ^t is the reflectance observed by the spaceborne sensor at instant *t*. Since we do not know a priori which pixels and instants are cloud-free, we apply Eq. 2 to a time-series of observed reflectances and we obtain a time series of possible ground reflectances, called apparent ground reflectances $\rho_\alpha{}^t$. The time-series is constructed by taking all images available for a month. Assuming that at a given location, the ground reflectance is less than the reflectance of any cloud and that the ground reflectance is constant throughout the month, the ground reflectance at this location is in principle the minimum value in this time-series. The time-series for a pixel is restricted to instants for which the sun is high enough above the horizon:

$$\theta_S \leq minimum(\, 2\, [\pi/2 - \theta_S^{noon}] / 3,\, 5\pi/18\,) \qquad (3)$$

where θ_S^{noon} is the angle observed at noon. The first and second minima are searched in this time series. Experience shows that the absolute minimum is subject to undetected defects in the original image or to other processes, such as shadows of clouds, which create artificially low ground reflectances, especially in desert areas, and is more variable than the second minimum. Therefore, we set the ground albedo ρ_g for this period to the second minimum. Note that this does not ensure that this value is the requested ground reflectance: it may be a cloud reflectance if all instants are cloudy or if ρ_g is larger than the lowest reflectances of clouds, or the shadow of a cloud or a minimum of ρ_g if the latter varies during the month. One way to palliate this shortcoming may be to consider the same time-series but in the thermal infrared range. The radiances observed in this range are a function of the temperature of the

object. If one assumes that the ground is warmer than any cloud, one may search the instant when temperature reaches its maximum and decide that ρ_g is equal to the reflectance for this instant. Another solution may be to search for local extreme in bidimensional space: low reflectance and high temperature.

In our case, only images in visible band were available. Before performing the search for ρ_g for every month, we perform this operation once for all for a time-series of images spanning from 1985 to 1990. Only images acquired at 1200 UTC were used; at that time most pixels are well sunlit. The resulting ground albedo was checked against typical values for soils (urban areas, vegetated fields), forests, deserts and water (Moussu et al., 1989) with the help of atlases and maps. Corrections to the ground albedo were brought manually if necessary; they concerned pixels which are the farthest from the nadir point of the satellite which is located in the equatorial plane at 0° in longitude or which are in the equatorial areas permanently covered by clouds. Thus, we created a map of ground albedo that include external knowledge and that is called reference map, ρ_g^{ref}. This map is used to control the ground reflectance assessed every month: ρ_g should be comprised in the interval [ρ_g^{ref}/2, 2 ρ_g^{ref}]. Otherwise, it is set to the corresponding threshold. The use of a reference map prevents the case of geographical areas that are under clouds for long periods, such as the equatorial belt or some parts of Northern Europe.

The authors are aware that this approach to the ground albedo is limited as already discussed by RLW. It cannot cope with the case of a sudden appearance of snow on the ground, a case which occur frequently in winter in Europe; the impact on the retrieval of the SSI is usually small because the sky is fully overcast but if not, the error in retrieval may be very large as it was the case in winter 2005. The assessment of the ground albedo may be improved by integrating the work of Zelenka (2003). In a similar way, one may consider shortening the period from one month to one week in order to deal with the rapid appearance of vegetation in Sahelian regions (Diabaté et al., 1989). Indeed, a trade-off should be found between the time requested to have a cloud-free instant for sure and the time scale of the rapid changes in albedo. Such an investigation has not yet been performed in our group; it is possible that the solution proposed for snow appearance may work in other cases.

Beyond these spectacular cases, one should note the importance of the assessment of the ground reflectance on the error in the assessment of the SSI. This is illustrated by a rough computation. If we restrict ourselves to the case where the clear-sky index ranges from clear (K_c =1) to slightly overcast (K_c =0.2), the equations of the method Heliosat-2 (see below) lead

to:

$K_c = 1 - [\rho_\alpha{}^t - \rho_g] / [\rho_{cloud} - \rho_g]$ (4)

where ρ_{cloud} is the reflectance of the very reflective clouds. Assume that the actual value of the ground reflectance is ρ_g. Its estimate, ρ_g*, differs by ε

$\rho_g^* = \rho_g + \varepsilon$ (5)

The estimate K_c* differs from the actual value:

$K_c^* = K_c + (\varepsilon / \rho_{cloud})$ (6)

and the estimate I* of the SSI:

$I^* = I + I_c\ (\varepsilon / \rho_{cloud})$ (7)

Eq. 7 shows that an error in ρ_g, positive or negative, leads to an error in I of the same sign. This error does not depend on the cloud cover. Its relative influence is the greatest for overcast skies. This error is actually not a bias because it depends upon ρ_{cloud} that is itself a function of θ_S and θ_v as explained below. Nevertheless, for a given pixel, i.e. a given θ_v, if we assume that θ_S exhibits small changes throughout the month for a given hour, one may consider this error as a bias in the SSI. Typical values for ε and ρ_{cloud} are respectively, 0.05 and 1.5. The error is then 0.03 times I_c. In the case of Northern Europe where clouds are very frequent, a typical clear-sky SSI is 300 W m^{-2} and I is 100 W m^{-2}; consequently, the error would be 9 W m^{-2}, i.e., 9% of I.

3.3 The reflectance of the very reflective clouds

RLW assessed the effective reflectance of very reflective clouds ρ_{eff} from drawings in Taylor and Stowe (1984a):

$\rho_{eff} = 0.85 - 0.13\ [1 - \exp(-4 \cos(\theta_S)^5]$ (8)

Note that a mistake was made in the corresponding equation in RLW (Eq. 8, 0.78 was written instead of 0.85). To compare the cloud reflectance to the ground reflectance, RLW define ρ_{cloud} as:

$\rho_{cloud} = [\rho_{eff} - \rho_{atm}] / T(\theta_S)\ T(\theta_v)$ (9)

with

$\rho_{cloud} > 0.2$, otherwise $\rho_{cloud} = 0.2$ and

$\rho_{cloud} < 2.24\ \rho_{eff}$, otherwise $\rho_{cloud} = 2.24\ \rho_{eff}$

The value 2.24 is the largest anisotropy factor observed by Taylor and Stowe (1984b) for the geometrical configuration sun-pixel-Meteosat and thick water cloud. A typical value for ρ_{cloud} is 1.5. As for ρ_g, we can assess the influence of an error in ρ_{cloud} on I. Assume that K_c is in the range [0.2, 1] and that ρ_{cloud} is much greater than ρ_g. Then, we can write:

$$K_c \approx 1 - (\rho_\alpha{}^t - \rho_g) / \rho_{cloud} \qquad (10)$$

Assume ρ_{cloud} is the actual value for very reflective clouds. Its estimate, ρ_{cloud}*, differs by a quantity δ such as:

$$\rho_{cloud}{}^* = \rho_{cloud} (1+ \delta) \qquad (11)$$

with $\delta \geq 0$ *or* < 0 *and* $ABS(\delta) << \rho_{cloud}$

where *ABS* means the absolute value. The estimate K_c* of K_c is:

$$K_c{}^* \approx 1 - (\rho_\alpha{}^t - \rho_g) / \rho_{cloud}{}^*$$

$$= 1 - (\rho_\alpha{}^t - \rho_g) / [\rho_{cloud} (1+ \delta)] \qquad (12)$$

$$K_c{}^* \approx 1 - [(\rho_\alpha{}^t - \rho_g) / \rho_{cloud}] (1- \delta)$$

$$\approx K_c + (1 - K_c) \delta \qquad (13)$$

The estimate I* of I is:

$$I^* = K_c{}^* I_c \approx K_c I_c + (1-K_c) \delta I_c$$

$$= I + (1-K_c) \delta I_c \qquad (14)$$

The error in I is $(1-K_c) \delta I_c$; it has the same sign that δ. It is equal to 0 when $K_c=1$. It increases as K_c decreases, i.e., as the sky is becoming cloudy. It may be very large as shown by the following numerical example. Assume $\delta = 0.25$ and $K_c = 0.2$. Then the error is equal to 20% of I_c. If we take the same case as before with I_c = 300 W m^{-2} and I = 100 W m^{-2}, the error amounts to 60 W m^{-2}, that is 60% of I.

3.4 The computation of the daily mean of SSI

For each pixel and each instant, a cloud index n^t is computed:

$$n^t = [\rho_\alpha{}^t - \rho_g{}^t] / [\rho_{cloud}{}^t - \rho_g{}^t] \qquad (15)$$

The cloud index is close to 0 when the observed reflectance is close to the ground reflectance, i.e., when the sky is clear. It can be negative if the sky is very clean, in which case $\rho_\alpha{}^t$ is smaller than $\rho_g{}^t$. The cloud index increases as the clouds are appearing. It can be greater than

1 for clouds that are considerably optically thick. Compared to RLW, we add several numerical constraints and the cloud index is computed as follows:

If $\rho_\alpha^{\,t} < 0.01$, $n^t = 0$

Else if $ABS(\rho_\alpha^{\,t} - \rho_g^{\,t}) < 0.01$, $n = 0$

Else if $ABS(\rho_{cloud}^{\,t} - \rho_g^{\,t}) < 0.10$, $n = 1.2$ *(an arbitrary large value)*

Else $n^t = [\rho_\alpha^{\,t} - \rho_g^{\,t}] / [\rho_{cloud}^{\,t} - \rho_g^{\,t}]$ *(16)*

If $n^t < -0.5$, $n^t = -0.5$

If $n^t > 1.5$, $n^t = 1.5$

An example of an image of cloud index is given in Fig. 2. The following relationship holds between n^t and K_c:

$$\begin{array}{rl} n^t < -0.2 & K_c = 1.2 \\ -0.2 < n^t < 0.8 & K_c = 1 - n^t \\ 0.8 < n^t < 1.1 & K_c = 2.0667 - 3.6667\, n^t + 1.6667 (n^t)^2 \\ n^t > 1.1 & K_c = 0.05 \end{array} \qquad (17)$$

Then, the SSI I^t is computed for this instant t by the means of Eq. 1. The daily mean of SSI I_d is computed from the N values of I^t available for that day:

$$I_d = \sum_{i=1}^{N} I^i \; / N \qquad (18)$$

At each instant in the summation, θ_S should be smaller than 75° for the clear-sky model to be valid. The larger N, the more accurate I_d. In our case, where B2 data are used, N ranges from 1 to 5.

Thus, the method Heliosat-2 converts satellite data into assessments of the daily mean of the SSI for each day. The accuracy of the method was assessed by RLW by processing high-resolution Meteosat images and comparing the derived SSI to measurements made in the meteorological networks in Europe. The results of RLW are reproduced in Table 1. Note that contrary to many similar works, these values are obtained by comparing the ground measurements to the estimated values for the single pixel containing the ground station with no spatial averaging.

3.5 The special case of the sun glitter over the ocean

The pattern of dancing highlights caused by the reflection of the sun from a water surface is called the sun glitter pattern. The surface of the ocean may be differentiated into small, mirror like facets. At spacecraft altitude, the reflecting facets are not individually resolved.

Therefore, the apparent radiance of the sea surface in any direction depends on the fraction of the area having the proper slope for specular reflection. The observed glitter pattern shows a radiance decreasing smoothly outward from its centre, since greater and therefore less frequent slopes are required for specular reflection as the distance from the centre increases (Wald and Monget, 1983a). This is illustrated in Fig. 1. When the wind speed increases, the roughness of the sea surface increases, the occurrence of large facet slopes increases and the pattern broadens with the level of radiance at the centre decreasing. The glitter pattern is centred on the specular point that is approximately defined as the pixel for which the satellite viewing and solar zenithal angles are equal and the difference of the azimuths of the sun and the satellite is equal to 180 ° (they are opposite). Far from the specular point, the ocean reflectance is approximately constant. In Fig. 1, the glitter pattern is visible in the middle of the image; the sun is at its zenith; the specular point is roughly southward of the nadir of the satellite.

Contrary to the usual case of ground reflectance, the reflectance of the ocean is highly variable with θ_S, θ_V and the difference in azimuth angles of the sun and sensor because of its non-Lambertian nature; it ranges from null values to values greater than cloud reflectances (Wald and Monget, 1983b). In addition, it depends upon the instantaneous wind speed at the surface. The approach adopted to assess the ground albedo is not effective in the case of the glitter pattern. It is suitable only outside this area. Another approach was designed within the glitter pattern. For practical reasons, it was decided to correct the cloud index in the glitter pattern instead of the reflectance. A window is defined centred on the specular point. The search for this point is limited to the area where it can be observed, i.e. between the latitudes 35° N and –35° S approximately, with θ_S and θ_V less than 40°. Otherwise, no correction is applied. The window is large enough to encompass the largest size of the glitter pattern: approximately 2000 km in radius. Only are considered the pixels known as belonging to the ocean. For each pixel in this window, if the cloud index is greater than 0.2, the sky is said cloudy and no correction is applied. Otherwise, a new window of 3 x 3 pixels is defined centred on the current pixel. One counts the number of pixels exhibiting cloud indices less than 0.2. If this number is strictly greater than 5 (60% of the total), the current pixel is considered as cloud-free and the cloud index is set to 0. Figure 2 shows the application of the method on the previous image (Fig. 1). The uncorrected map exhibits cloud indices that are too large in the glitter pattern. They are mistaken as clouds and the resulting SSI will be too low. Once corrected, the cloud indices offer values that are similar to the other cloudless parts of the ocean. The cloudy pixels are not affected by the correction.

4. THE B2 DATA SET USED

The B2 data set is produced from Meteosat images by firstly performing a time sampling that reduces the frequency of observation to the standard meteorological synoptic 3-h intervals, starting at 0000 UTC. The Earth is scanned by the first series of Meteosat satellites (Meteosat-1 to –7) in approximately 25 minutes. An image acquired at, say 1200 UTC is actually acquired between 1130 and 1155 UTC. The time used in the computations is the actual acquisition time for this particular pixel. Secondly, the higher-resolution data in the visible-channel are averaged to match the lower resolution of infrared-channel data (i.e. an image of 2500 x 2500 pixels with a resolution of 5 km). Finally, a spatial sampling is performed by taking 1 pixel over 6 in each direction, starting with the south-easternmost pixel. The effects of the temporal sampling on the reconstruction of the daily mean of SSI were discussed by England and Hunt (1984); they found that the accuracy decreases as the sampling rate decreases. Pinker and Laszlo (1991) investigated the effects of spatial sampling: the estimated SSIs differed by 9% depending upon the sampling. Consequently, we expect a lower accuracy for the SSI derived from B2 data than for those derived from high-resolution images (Table 1).

The B2 data set spans from 1994 to 1997. It covers the whole field of view of Meteosat, i.e. Europe, Africa and the Atlantic Ocean. Meteosat data were converted into radiances using the calibration coefficients proposed by Rigollier et al. (2002). Each image of radiances was processed by the means of the method Heliosat-2. Estimates of the daily mean of SSI are thus obtained for each B2 pixel. There are 118500 such pixels. The assessment of the SSI for any geographical site $\boldsymbol{P}$ is made by the means of a linear interpolator of gravity-type applied to the nine nearest B2 pixels $\boldsymbol{X_j}$ ($j=1...9$):

$$I_d(\boldsymbol{P}) = \sum_{j=1}^{9} w_j \mathrm{I}_d(X_j) \qquad (19)$$

where $I_d(\boldsymbol{X_j})$ denotes the SSI at B2 pixel $\boldsymbol{X_j}$. The weights w_j are defined by the inverse of a squared distance d_j separating $\boldsymbol{P}$ and each $\boldsymbol{X_j}$:

$$w_j = (1 / d_j^2) \sum_{k=1}^{9} \mathrm{d}_k^2 \qquad (20)$$

The geodetic distance between $\boldsymbol{P}$ and $\boldsymbol{X_j}$ ranges from 20 to 80 km. After several comparisons with the nearest neighbour and the geodetic distance, we selected the effective distance

proposed by Lefèvre et al. (2002) and already used by Diabaté et al. (2004) for mapping solar radiation climate in Africa. This effective distance d_{eff} takes into account latitudinal and orographic effects and offers a better accuracy:

$$(d_{eff}^{j})^2 = (f_{NS}^{j})^2 \left((d_{geo}^{j})^2 + f_{oro}^{\,2} (\delta h^{j})^2\right) \qquad (21)$$

$$\text{with } (f_{NS}^{j}) = 1 + 0.3\, ABS(\Phi_P - \Phi_{Xj})\, [1 + (\sin\Phi_P + \sin\Phi_{Xj}) / 2]$$

where (d_{geo}^{j}) is the geodetic distance between $\boldsymbol{P}$ and $\boldsymbol{X}_j$ in km, latitudes Φ_P and Φ_{Xj} are expressed in degrees, counted positive from the equatorial plane northwards and negative southwards, (δh^{j}) is the difference in elevation between $\boldsymbol{P}$ and $\boldsymbol{X}_j$, expressed in km, and f_{oro} is equal to 500.

5. COMPARING GROUND MEASUREMENTS TO SATELLITE-DERIVED ASSESSMENTS

Ground measurements were assembled to assess the B2-derived SSI. They consist in daily irradiation collected by the meteorological networks in Europe and Africa. Fifty-five stations are available for Europe, covering July 1994 to June 1995, and located in flat areas of low altitude (Table 2). Thirty-five stations are available for Africa, covering four years, spanning from January 1994 to December 1997 (Table 3). The quality of the ground data measurements of the global irradiation was controlled by the means of a Web tool in order to remove suspicious data (see at www.helioclim.net, Geiger et al., 2002). Following the ISO standard (1995), we compute the difference: estimated-measured for each day, and summarize these differences by the bias, the root mean square difference (RMSD) and the correlation coefficient. We performed this operation for daily and monthly means of SSI, each region and each year. The monthly means are computed from daily values; we kept only days that are coincident in both time-series and declared a monthly mean valid only if it is made from at least 60% of valid daily mean of SSI, i.e., 17 to 18 days per month.

The authors consider that the result of the interpolation procedure is equivalent to an assessment made over a pixel containing the site $\boldsymbol{P}$. Therefore, the two time-series to compare are different in nature: one is made of pin-point measurements, the other of space-averaged assessments. Accordingly, a discrepancy is expected because of the natural variability of the SSI in space; Zelenka et al. (1999) found within a pixel a standard deviation of 10-15% relative to the mean SSI.

Table 4 reports results for the daily mean of SSI. The correlation coefficient is high in all cases and larger than 0.9: day-to-day variations are well reproduced. Looking for Europe, one note that the bias and RMSD are close to those reported in Table 1 for high-resolution imagery. The bias is negative, which means an underestimation of the SSI. As expected, the bias and RMSD are greater than those found by RLW with high resolution images, and the differences in RMSD are in agreement with the findings of England and Hunt (1984) and Pinker and Laszlo (1991). As a whole, the bias is negative for Europe (underestimation) and positive for Africa (overestimation). The bias varies from one year to another. It is of order of a few percent in relative value though a large value of 9% was found for Europe in 1995. The relative RMSD ranges between 15 and 25%. The largest relative difference is attained for Europe in 1995 and is related to the largest relative bias.

If all data are merged together, the observed mean value is 202 W m^{-2}, and with 48490 observations spanning from 1994 to 1997, we found a bias of 1 W m^{-2}, which is very low; the RMSD is 35 W m^{-2} (17%).

However, the picture is not as simple if we consider sites individually. The bias may range from –15 W m^{-2} (Easthampstead, United Kingdom) to 32 W m^{-2} (Wenchi, Ghana). Though for Europe, the bias is negative, it is equal to 8 W m^{-2} in Bergen (Norway) for 1994-1995. On the contrary, we found a bias of –13 W m^{-2} in Bahtim (Egypt) or Nampula (Mozambique) while the overall bias for Africa is positive. The study indicates that the relative bias and relative RMSD are usually low for clear skies and degrade for overcast skies but this is only a trend as it will be illustrated later. As a whole the greater the irradiance, the greater the bias in absolute value and the greater the RMSD. This was observed by RLW (Table 1). For Europe, it means that error in January is less than in July. Combined to that, one may observe in general a seasonal variation in error at a given site (Figs 3 to 6). This is not true for all sites (Fig. 3). The sun elevation plays a role; an overestimation of the SSI is often observed for low sun elevation (large θ_S). One of the possible reasons is the decrease in the number N of hourly estimates for constructing the daily mean (Eq. 18). The influence of θ_V is not noticeable. Nevertheless, it is difficult to draw definite conclusions as there are several quantities in the method Heliosat-2 that influence the results as already discussed and illustrated below.

The correlation coefficient for monthly mean of SSI is higher than for the daily mean of SSI (Table 5). The relative RMSD ranges between 11 to 13% with an exception at 16% for Europe in 1995. If all data are merged together (1584 samples), the bias is 1 W m^{-2} and the RMSD is 25 W m^{-2} (12%), notably less than for the daily mean of SSI.

We selected four stations to illustrate the quality and drawbacks of the method. These four

stations are representative of a radiation climate according to ESRA (2000) and Diabaté et al. (2004). Braunschweig, in Germany, is situated at the northern foot of the central German uplands. The station is influenced partly by maritime but more by continental air masses depending on the actual weather conditions. Classified with the climatic types of Trewartha (1954), the area has a climate coded as Cb: rainy climate with mild winters, coldest month with mean temperatures ranging between 0 and 8° C, warmest month with mean temperatures less than 22° C. The average clearness index *KT* is reported for each month in Table 6. Wenchi is located in Ghana in the equatorial zone, North of the Gulf of Guinea. The climate is coded Aw, which means a rainy climate with no winter and the driest months in boreal winter. The temperature of the coolest month is above 18° C. *KT* is almost constant from November to May at approximately 0.45 (Table 6). Then it decreases to 0.32 in August and then increases again. Maputo (Mozambique) is located on the Southeast coast of Africa, in the Limpopo plain. The climate is similar to that of Wenchi (code Aw) with the driest months in austral winter (June-August). It is characterized by *KT* almost constant during the year, ranging between 0.53 and 0.59, with a maximum in austral winter (Table 6). El Arish is in the arid Sinai Peninsula. Climate is that of a warm dry desert (code BWh). The sky is very clear in boreal summer: *KT* is larger than 0.65 (Table 6). The lowest values of 0.55 are attained in November and December.

Figure 3 displays the monthly means of SSI observed and assessed at Braunschweig. Table 7 reports on the statistics for this site. The underestimation is important: -13 W m^{-2}; the RMSD is slightly greater than the bias, in absolute value; the correlation coefficient is very large: 0.99. The assessed SSI reproduces quite well the variations of the observed SSI, except for July 1995. The underestimation may be explained by *TL* slightly too large (i.e. I_c too small) from January to June as explained by Equation 1. The outlier seen for July 1995 is due to an underestimation of ρ_g; it may be due to an optically thin cloud that decreases the reflectance of the ground observed by the sensor. Equation 7 shows that an underestimation of ρ_g leads to an underestimation of the SSI. For the site Wenchi (Fig. 4, Table 7), the agreement is not good. The correlation coefficient is lower than usual: 0.77. There is a large overestimation from November to April that can be explained by too low values of *TL* (i.e. I_c too large). The agreement in austral winter (June-August) is fairly good in 1994 and very good in 1995 though the sky is very cloudy during this period. This illustrates the fact that though the relative error usually increases when the cloud cover increases, it is not systematically the case. The agreement is very good for the site Maputo (Fig. 5, Table 7). The correlation coefficient is very large: 0.96; the bias and RMSD are small. A large underestimation (-50 W

m^{-2}) is observed in February 1994. As the SSI is very similar from one year to another and as the agreement is good for February 1995, we conclude that *TL* is correct and that the discrepancy in February 1994 is likely due to an underestimation of ρ_g. The site El Arish exhibits one of the best agreements (Fig. 6 and Table 7). The correlation coefficient is 1.00 and the bias is low. One may observe an overestimation in June-July and an underestimation in November-December for both years. As the SSI is constant from one year to another, we may conclude that *TL* should be modified for these 4 months.

6. CONCLUSION

With an observed mean value of 202 W m^{-2}, we found a bias of 1 W m^{-2} and a RMSD of 35 W m^{-2} (17%) for daily mean of SSI. This is slightly worse than the accuracy reported for the data set Medias (1996) that deals with the Mediterranean basin. The Medias data set was constructed using original Meteosat data, with a temporal sampling of 0.5 h and a degraded spatial resolution of 0.2° of arc angle (approximately 20 km). A comparison made against 9116 observations made in France in 1994, with a mean value of 145 W m^{-2}, results into a bias of -1 W m^{-2} and a RMSD of 18 W m^{-2} (13%). These values are similar to those found by RLW; the differences with the present study are related to the difference in temporal sampling (0.5 h versus 3 h) and to the use of spatial averaging in the case of the Medias data set.
As for the monthly mean of SSI, we found of course a similar bias of 1 W m^{-2} and a RMSD of 25 W m^{-2} (12%). This is close to the accuracy of the SRB data set. Comparing irradiance on pixel of 280 km in size and 13356 measurements made in the Global Energy Balance Archive (GEBA) from July 1983 to June 1991, Darnell et al. (1996) report a bias of -5 W m^{-2} and a RMSD of 24 W m^{-2}.
The results clearly demonstrate that the combination of the images in reduced format B2 and the method Heliosat-2 offers enough accuracy for creating a climatological database of the daily mean SSI over large areas with a grid cell of about 5' of arc angle in size (approximately 10 km at mid-latitude). It is concluded that such B2 data can be used in a reliable way in producing time-series of SSI for Europe, Africa and the Atlantic Ocean, except for very high latitudes greater than approximately 65°. Though not tested, the authors believe that the conclusions hold for other parts of the world.
An effort has been launched at Ecole des Mines de Paris / Armines for creating and managing a database, called HelioClim-1, that contains daily mean of SSI for the field of view of

Meteosat for a period beginning 1st January 1985 (Cros, 2004; Cros et al., 2004). The data are accessible via the SoDa Web site (http://www.soda-is.com). The database comprises the equivalence of 118500 measuring pseudo-stations (the B2 pixels). Given any geographical location, the Web server performs an on-line spatial interpolation using the nine surrounding pseudo-stations to deliver a time-series of irradiance for this location. Figure 7 displays an example of a map constructed from this database. It represents the monthly mean of SSI for France and surroundings in August 2003. The grey scale was constructed in order to display best the spatial features and to demonstrate that features of scale of 50 km or greater are well represented.

In this geographical area (Europe, Africa), there are about 410 stations measuring the global radiation on a daily basis in the WMO network (source WMO Web site www.wmo.ch, 3 May 2002). These 410 stations hardly compare to the 118500 pseudo-stations. There are in addition 1910 WMO stations measuring the sunshine duration; the latter can be converted into global radiation for monthly means if the parameters of the Angstrom relation between both quantities are known. Even so, this number cannot compete against the capabilities offered by the satellite, even in reduced format.

ACKNOWLEDGMENTS

The World Radiation Data Center (WRDC) provided the data for Africa. The meteorological offices from Belgium, France, Germany, Hungary, South Africa, Spain and United Kingdom have kindly provided the measurements of global irradiation at no or low cost. They are thanked for their support. Thanks to Jan Olseth for the data for Bergen, Norway. The B2 data were offered at reproduction cost by Eumetsat. Many thanks go to the anonymous reviewers whose comments help in greatly improving the quality of this article. This work was partly supported by the European Commission, under the Information Society Technology Programme (SoDa project IST-1999-12245) and partly by the Service de Coopération et d'Action Culturelle de l'Ambassade de France in Mali.

REFERENCES

AGSRA, Australian Global Solar Radiation Archive server, on-line at www.bom.gov.au, 2003.

Anonymous, 1996. The Meteosat system, Eumetsat publ. #TD05, Eumetsat, Darmstadt,

Germany.
Ba, M., Nicholson, S., Frouin, R., 2001. Satellite-derived surface radiation budget over the African continent. Part II: Climatologies of the various components. Journal of Climate, 14, 60-76.
Cano, D., Monget, J.-M., Albuisson, M., Guillard, H., Regas, N., Wald, L., 1986. A method for the determination of the global solar radiation from meteorological satellite data. Solar Energy, 37, 31-39.
Cros, S., 2004. Création d'une climatologie du rayonnement solaire incident en ondes courtes à l'aide d'images satellitales. Thèse de Doctorat en Energétique, Ecole des Mines de Paris, Paris, France, 157 pp.
Cros, S., Albuisson, M., Lefèvre, M., Rigollier, C., Wald, L., 2004. HelioClim: a long-term database on solar radiation for Europe and Africa. In Proceedings of Eurosun 2004, published by PSE GmbH, Freiburg, Germany, pp. 916-920(3).
Darnell, W.L., Staylor, W.F., Ritchey, N.A., Gupta, S.K., Wilber, A.C., 1996. Surface radiation budget: a long-term global dataset of shortwave and longwave fluxes, American Geophysical Union. Available from: http://www.agu.org/eos_elec/95206e.html.
Diabaté, L., Michaud-Regas., N., Wald, L., 1989. Mapping the ground albedo of Western Africa and its time evolution during 1984 using Meteosat visible data. Remote Sensing of Environment, 27, 3, 211-222.
Diabaté, L., Blanc, Ph., Wald, L., 2004. Solar radiation climate in Africa. Solar Energy, 76, 733-744.
England, C.F., Hunt, G.E., 1984. A study of the errors due to temporal sampling of the earth's radiation budget, Tellus, 36B, 303-316.
ESRA, 2000. European Solar Radiation Atlas, fourth ed., includ. CD-ROM. Edited by Greif, J., and K. Scharmer. Scientific advisors: R. Dogniaux, J. K. Page. Authors: L. Wald, M. Albuisson, G. Czeplak, B. Bourges, R. Aguiar, H. Lund, A. Joukoff, U. Terzenbach, H. G. Beyer, E. P. Borisenko. Published for the Commission of the European Communities by Presses de l'Ecole, Ecole des Mines de Paris, Paris, France.
Geiger, M., Diabaté, L., Ménard, L., Wald, L., 2002. A web service for controlling the quality of measurements of global solar irradiation. Solar Energy, 73, 475-480.
ISO, 1995. Guide to the Expression of Uncertainty in Measurement, first ed. International Organization for Standardization, Geneva, Switzerland.
Lefèvre, M., Remund, J., Albuisson, M., Wald, L., 2002. Study of effective distances for interpolation schemes in meteorology. Geophysical Research Abstracts, 4, April 2002,

EGS02-A-03429, European Geophysical Society.
Medias, 1996. Mediterranean Oceanic Database – Satellite Data and Meteorological Model Outputs. 2 CD-ROMs, produced by Meteo-France, CNES, IFREMER, CLS, ESA and GRGS. Published by Medias-France, CNES, Toulouse, France.
Moussu, G., Diabaté, L., Obrecht, D., Wald, L., 1989. A method for the mapping of the apparent ground brightness using visible images from geostationary satellites. International Journal of Remote Sensing, 10, 7, 1207-1225.
Pastre, C., 1981. Développement d'une méthode de détermination du rayonnement solaire global à partir des données Meteosat. La Météorologie, VIe série N°24, mars.
Perez, R., Seals, R., Zelenka, A., 1997. Comparing satellite remote sensing and ground network measurements for the production of site/time specific irradiance data. Solar Energy, 60, 89-96.
Pinker, R. T., Laszlo, I., 1991. Effects of spatial sampling of satellite data on derived surface solar irradiance. Journal of Atmospheric and Oceanic Technology, 8, 96-107.
Raschke, E., Gratzki, A., Rieland, M., 1987. Estimates of global radiation at the ground from the reduced data sets of the International Satellite Cloud Climatology Project. Journal of Climate, 7, 205-213, 1987.
Raschke, E., Stuhlmann, R., Palz, W., Steemers, T.C., 1991. Solar Radiation Atlas of Africa, published for the Commission of the European Communities by A. A. Balkema, ISBN 90-54-5410, 155 pp.
Remund, J., Wald, L., Lefèvre, M., Ranchin, T., Page, J., 2003. Worldwide Linke turbidity information. Proceedings of ISES Solar World Congress, 16-19 June 2003, Göteborg, Sweden, CD-ROM published by International Solar Energy Society.
Rigollier, C., Bauer, O., Wald, L., 2000. On the clear sky model of the 4th European Solar Radiation Atlas with respect to the Heliosat method. Solar Energy, 68, 33-48.
Rigollier, C., Lefèvre, M., Blanc, Ph., Wald, L., 2002. The operational calibration of images taken in the visible channel of the Meteosat-series of satellites. Journal of Atmospheric and Oceanic Technology, 19, 1285-1293.
Rigollier, C., Lefèvre, M., Wald, L., 2004. The method Heliosat-2 for deriving shortwave solar radiation from satellite images. Solar Energy, 77, 159-169.
Rimoczi-Paal, A., Kerenyi, J., Mika, J., Randriamampianina, R., Dobi, I., Imecs, Z., Szentimrey, T., 1999. Mapping daily and monthly radiation components using Meteosat data. Advanced Space Research, 24, 967-970.
Schiffer, R., Rossow, W.B., 1985. ISCCP global radiance data set: a new resource for climate

research. Bulletin of American Meteorological Society, 66, 1498-1503.
Stuhlmann, R., Rieland, M., Raschke, E., 1990. An improvement of the IGMK model to derive total and diffuse solar radiation at the surface from satellite data. Journal of Applied Meteorology, 29, 596-603.
Taylor, V.R., Stowe, L.L., 1984a. Reflectance characteristics of uniform Earth and cloud surfaces derived from Nimbus 7 ERB. Journal of Geophysical Research, 89, 4987-4996.
Taylor, V.R., Stowe, L.L., 1984b. Atlas of reflectance patterns for uniform Earth and cloud surfaces (Nimbus 7 ERB – 61 days), NOAA Technical Report NESDIS 10, July 1984, Washington, DC, USA.
TerrainBase, 1995. Worldwide Digital Terrain Data, Documentation Manual, CD-ROM Release 1.0, April 1995, NOAA, National Geophysical Data Center, Boulder, Colorado, USA.
Trewartha, G. T., 1954. An Introduction to Climate. 3rd ed. McGraw Hill Book Co.
Tuzet, A., Möser, W., Raschke, E., 1984. Estimating global solar radiation at the surface from Meteosat data in the Sahel region. Journal of Atmospheric Research, 18, 31-39.
Wald, L., Monget, J.-M., 1983a. Sea surface winds from sun glitter observations. Journal of Geophysical Research, 88, C4, 2547-2555.
Wald, L., Monget, J.-M., 1983b. Remote sensing of the sea-state using the 0.8-1.1 microns channel. *International Journal of Remote Sensing*, 4, 2, 433-446. Comments by P. Koepke and reply, 6, 5, 787-799, 1985.
Whitlock, C.H., Charlock, T.P., Staylor, W.F., Pinker, R.T., Laszlo, I., Ohmura, A., Gilgen, H., Konzelman, T., DiPasquale, R.C., Moats, C.D., LeCroy, S.R., Ritchey, N.A., 1995. First global WCRP shortwave surface radiation budget dataset. Bulletin of American Meteorological Society, 76, 905-922.
Zelenka, A., Czeplak, G., d'Agostino, V., Josefson, W., Maxwell, E., Perez, R., 1992. Techniques for supplementing solar radiation network data, Technical Report, International Energy Agency, # IEA-SHCP-9D-1, Swiss Meteorological Institute, Krahbuhlstrasse, 58, CH-8044 Zurich, Switzerland.
Zelenka, A., Perez, R., Seals, R., Renné, D., 1999. Effective accuracy of satellite-derived hourly irradiances. Theoretical and Applied Climatology, 62, 199-207.
Zelenka, A., 2003. Progress in estimating insolation over snow covered mountains with Meteosat VIS-channel: a time series approach. In Proceedings of the 3rd Workshop on Satellites for Solar Energy, March 19-21, 2003. University of Geneva, Switzerland.

TABLES CAPTIONS

Table 1. Results of the comparison between Heliosat-2 derived assessments and ground measurements of daily mean of SSI (in W m^{-2}) as reported by Rigollier et al. (2004) for high-resolution Meteosat images. RMSD: root mean square difference.

Table 2. List of the 55 stations used in Europe. The period is July 1994 – June 1995.

Table 3. List of the 35 stations used in Africa. All cover the period 1994 - 1997 except the two of South Africa (1994-1995)

Table 4. Results of the comparison between B2-derived assessments and ground measurements of daily mean of SSI (in W m^{-2}). The bias and the RMSD are also expressed in percent of the mean value.

Table 5. As Table 4, but for monthly mean of SSI.

Table 6. Typical values of the clearness index *KT* for the 4 sites and each month. Sources: ESRA (2000) and Diabaté et al. (2004).

Table 7. As Table 5, but for four sites.

Information type	*Month*	*Observed mean value*	*Bias*	*RMSD*	*Correlation coefficient*	*Number of observations*
Daily mean	Jan 95	41	2 (5%)	8 (20%)	0.95	344
	Apr 95	140	-7 (-5%)	22 (16%)	0.95	1044
	Jul 94	242	-6 (-2%)	24 (10%)	0.94	887
Monthly mean	Jan 95	37	5 (+14%)	9 (24%)	0.88	20
	Apr 95	140	-7 (-5%)	10 (7%)	0.97	35
	Jul 94	241	-8 (-3%)	13 (5%)	0.92	34

Table 1.

Station name	*WMO id.*	*Latitude*	*Longitude*	*Altitude*	*Country*
Melle	6430	50.98	3.83	17	Belgium
St. Hubert	6476	50.03	5.40	556	Belgium
Uccle	6447	50.80	4.35	100	Belgium
Agen	7524	44.18	0.60	59	France
Caen	7027	49.18	-0.45	64	France
Carcassonne	7635	43.22	2.32	130	France
La Roche sur Yon	7306	46.70	-1.05	90	France
Rennes	-	48.05	-2.00	88	France
Reims	7070	49.30	4.03	95	France
Port de Bouc	-	43.39	4.18	50	France
Bourges	7255	47.07	2.37	161	France
Captieux	7517	44.18	-0.28	132	France
Limoges	7434	45.87	1.18	402	France
Macon	7385	46.30	4.80	216	France
Perpignan	7747	42.73	2.87	43	France
St. Quentin	7061	49.82	3.20	98	France
Bocholt	10406	51.83	6.53	24	Germany
Braunschweig	10348	52.30	10.45	83	Germany
Bremen	10224	53.05	8.80	24	Germany
Bonn - Friesdorf	10517	50.70	7.15	65	Germany
Coburg	10671	50.28	10.98	331	Germany
Kassel	10438	51.30	9.45	237	Germany
Dresden - Wahnsdorf	10486	51.12	13.68	246	Germany
Nuernberg	10763	49.50	11.08	312	Germany
Neubrandenburg	10280	53.55	13.20	73	Germany
Osnabrueck	10317	52.25	8.05	104	Germany
Potsdam	10378	52.37	13.08	107	Germany
Hamburg - Sasel	10141	53.65	10.12	49	Germany
Seehausen	10261	52.90	11.73	21	Germany
Saarbruecken	10708	49.22	7.12	325	Germany
Stuttgart	10739	48.83	9.20	318	Germany
Trier	10609	49.75	6.67	278	Germany
Weimar	10555	50.98	11.32	275	Germany
Weihenstephan	10863	48.40	11.70	472	Germany
Wuerzburg	10655	49.77	9.97	275	Germany
Budapest / Lorinc	12843	47.43	19.18	138	Hungary
Bergen	1316	60.40	5.32	41	Norway
Oviedo	8015	43.35	-5.87	335	Spain
Valladolid	8141	41.65	-4.77	734	Spain
Caceres	8261	39.47	-6.33	405	Spain
Murcia	8430	38.00	-1.17	61	Spain
Toledo	8272	39.88	-4.05	515	Spain
Madrid Universidad	8220	40.45	-3.72	664	Spain
Aviemore	3063	57.20	-3.83	220	United Kingdom
Easthampstead / Bracknell	3763	51.38	-0.78	73	United Kingdom
Eskdalemuir	3162	55.32	-3.20	242	United Kingdom
Aboyne	3080	57.08	-2.83	140	United Kingdom
Altnaharra	3044	58.28	-4.43	81	United Kingdom
Drungans	3155	55.62	-3.73	245	United Kingdom
Loch Glascanoch	3031	57.72	-4.88	265	United Kingdom
Kenley Airfield	3781	51.30	-0.08	170	United Kingdom
Saint Angelo	3903	54.40	-7.65	47	United Kingdom
Bedford	3560	52.22	-0.48	85	United Kingdom
Church Lawford	3544	52.36	-1.33	107	United Kingdom
Pershore	3529	52.15	-2.03	65	United Kingdom

Table 2.

Station name	WMO id.	Latitude	Longitude	Altitude	Country
Tamanrasset	60680	22.80	5.43	1364	Algeria
Sidi Barrani	62301	31.60	26.00	26	Egypt
Mersa Matruh	62306	31.33	27.22	38	Egypt
Rafah	62335	31.20	34.20	73	Egypt
El Arish	62337	31.08	33.82	32	Egypt
Tahrir	62345	30.65	30.70	19	Egypt
Bahtim	62369	30.13	31.25	17	Egypt
Cairo	62371	30.08	31.28	26	Egypt
Asyut	62392	27.20	31.17	52	Egypt
Aswan	62414	23.97	32.78	192	Egypt
Kharga	62435	25.45	30.53	70	Egypt
Bole	65416	9.03	-2.48	299	Ghana
Wenchi	65432	7.75	-2.10	339	Ghana
Axim	65465	4.87	-2.23	38	Ghana
Casablanca	60155	33.57	-7.67	57	Morocco
Pemba	67215	-12.98	40.53	49	Mozambique
Lichinga	67217	-13.30	3.52	1364	Mozambique
Nampula	67237	-15.10	39.28	438	Mozambique
Tete	67261	-16.18	33.58	123	Mozambique
Chimoio	67295	-19.12	33.47	731	Mozambique
Beira	67297	-19.80	34.90	10	Mozambique
Inhambane	67323	-23.87	35.38	14	Mozambique
Maputo	67341	-25.97	32.60	70	Mozambique
Chokwe	67397	-24.52	33.00	33	Mozambique
Maniquenique	67398	-24.73	33.53	13	Mozambique
Umbeluzi	673412	-25.95	32.38	12	Mozambique
Cape Town	68816	-33.96	18.60	46	South Africa
Pretoria	68262	-25.73	28.18	1310	South Africa
Arrecife	60040	28.95	-13.60	20	Spain
Mellilla	60338	35.28	-2.95	55	Spain
Sidi Bou Said	60715	36.87	10.23	127	Tunisia
Mansa	67461	-11.10	28.85	1384	Zambia
Lusaka	67666	-14.45	28.47	1280	Zambia
Harare	67774	-17.83	31.02	1471	Zimbabwe
Bulawayo	67964	-20.15	28.62	1343	Zimbabwe

Table 3.

	Mean value	Bias (relative)	RMSD (relative)	Correlation coefficient	Number of observations
1994 - Europe	137	-5 (-3%)	30 (22 %)	0.94	5843
1994 - Africa	229	0 (0 %)	34 (15 %)	0.90	8470
1994 - All	191	-2 (-1 %)	33 (17 %)	0.94	14813
1995 - Europe	148	-14 (-9 %)	36 (25 %)	0.93	6858
1995 - Africa	224	5 (2 %)	34 (15 %)	0.90	9778
1995 - All	193	-3 (-1 %)	35 (18 %)	0.93	16636
1996 - Africa	219	7 (3 %)	36 (16 %)	0.89	9399
1997 - Africa	218	8 (4 %)	38 (17 %)	0.89	8142

Table 4.

	Mean value	Bias (relative)	RMSD (relative)	Correlation coefficient	Number of observations
1994 - Europe	147	-6 (-4 %)	17 (12 %)	0.97	172
1994 - Africa	228	-1 (0 %)	24 (11%)	0.92	280
1994 - All	197	-2 (-1 %)	22 (11 %)	0.96	452
1995 - Europe	149	-14 (-9 %)	24 (16 %)	0.95	462
1995 - Africa	224	5 (2 %)	24 (11 %)	0.92	322
1995 - All	193	-3 (-2 %)	24 (12 %)	0.95	553
1996 - Africa	218	7 (3 %)	27 (12 %)	0.90	310
1997 - Africa	219	8 (4 %)	29 (13 %)	0.90	269

Table 5.

Station Name	Jan.	Feb.	Mar.	Apr.	May	Jun.	Jul.	Aug.	Sep.	Oct.	Nov.	Dec.
Braunschweig	0.30	0.35	0.37	0.43	0.47	0.42	0.45	0.45	0.40	0.37	0.31	0.26
Wenchi	0.45	0.49	0.47	0.44	0.44	0.39	0.35	0.31	0.34	0.43	0.49	0.44
Maputo	0.57	0.59	0.57	0.58	0.58	0.61	0.60	0.60	0.58	0.52	0.51	0.57
El Arish	0.58	0.62	0.63	0.64	0.66	0.68	0.66	0.65	0.62	0.58	0.55	0.56

Table 6.

		Braunschweig	Wenchi	Maputo	El Arish
1994	Mean value	148	172	227	232
	Bias (relative)	-13 (–9%)	32 (18%)	-6 (-3%)	5 (2%)
	RMSD (relative)	15 (10%)	44 (25%)	16 (7%)	12 (5%)
	Coeff. correl.	0.99	0.77	0.96	1.00
1995	Mean value	136	181	216	236
	Bias (relative)	-31 (-23%)	29 (16%)	-1 (-1%)	5 (2%)
	RMSD (relative)	37 (27%)	39 (22%)	10 (4%)	17 (7%)
	Coeff. correl.	0.97	0.77	0.98	0.99
1994-1995	Mean value	142	176	221	234
	Bias (relative)	-23 (-16%)	30 (17%)	-4 (–2%)	5 (2%)
	RMSD (relative)	29 (21%)	42 (24%)	13 (6%)	15 (6%)
	Coeff. correl.	0.97	0.76	0.99	1.00

Table 7.

FIGURES CAPTIONS

Figure 1. Meteosat visible image, taken on 1/1/1994, at 1200 UTC in B2 format. Reflectances increase from black to white. The satellite is located above the Gulf of Guinea. Note the circular clear pattern in this Gulf, at the centre of the image, partly covered by clouds. It is caused by the reflection of the Sun at the surface of the ocean.

Figure 2. Map of the cloud index n for the image shown in Figure 1. n increases from black to white. Only are represented pixels for which θ_V is less than 75°. The dark area is not processed because θ_S is greater than 75° for these pixels. The left image is not corrected for the glitter effects. The circle indicates the glitter pattern. Right: corrected for glitter.

Figure 3. Monthly mean of SSI during the years 1994 and 1995 as measured by a pyranometer at ground (continuous line) and assessed from satellite observation (dotted line), for the site of Braunschweig. Note that ground measurements were available from July 1994 to June 995 for this site.

Figure 4. As Fig. 3, but for the site Wenchi.

Figure 5. As Fig. 3, but for the site Maputo.

Figure 6. As Fig. 3, but for the site El Arish.

Figure 7. Example of a map constructed from the database HelioClim-1. It represents the monthly mean of SSI in August 2003 in W m^{-2}. The grey scale was constructed to enhance spatial features.

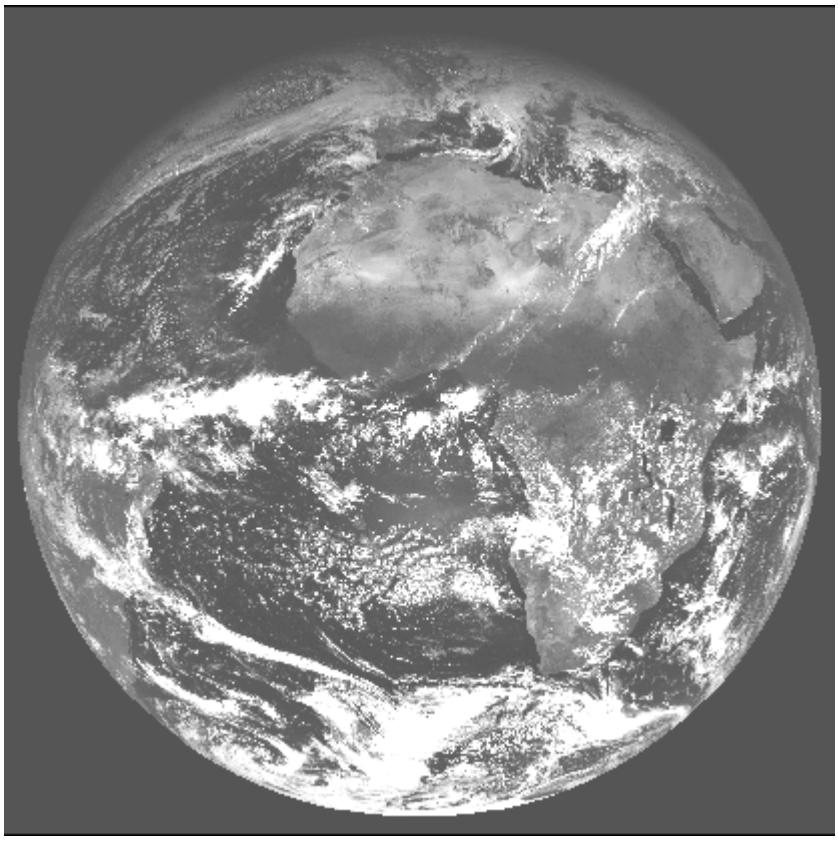

Figure 1.

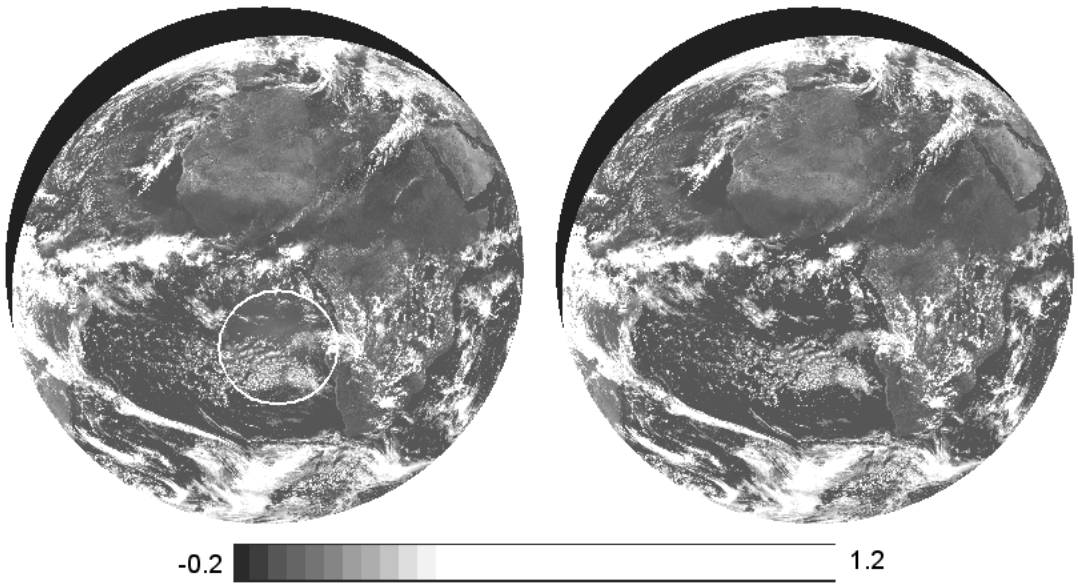

Figure 2.

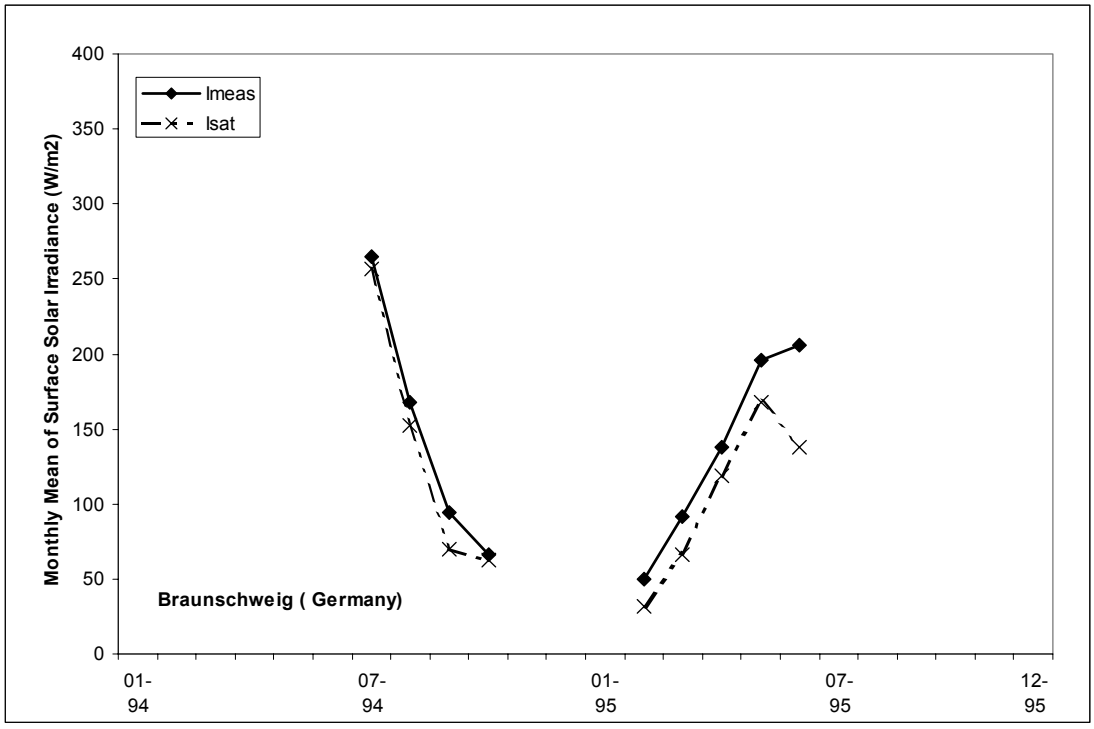

Figure 3.

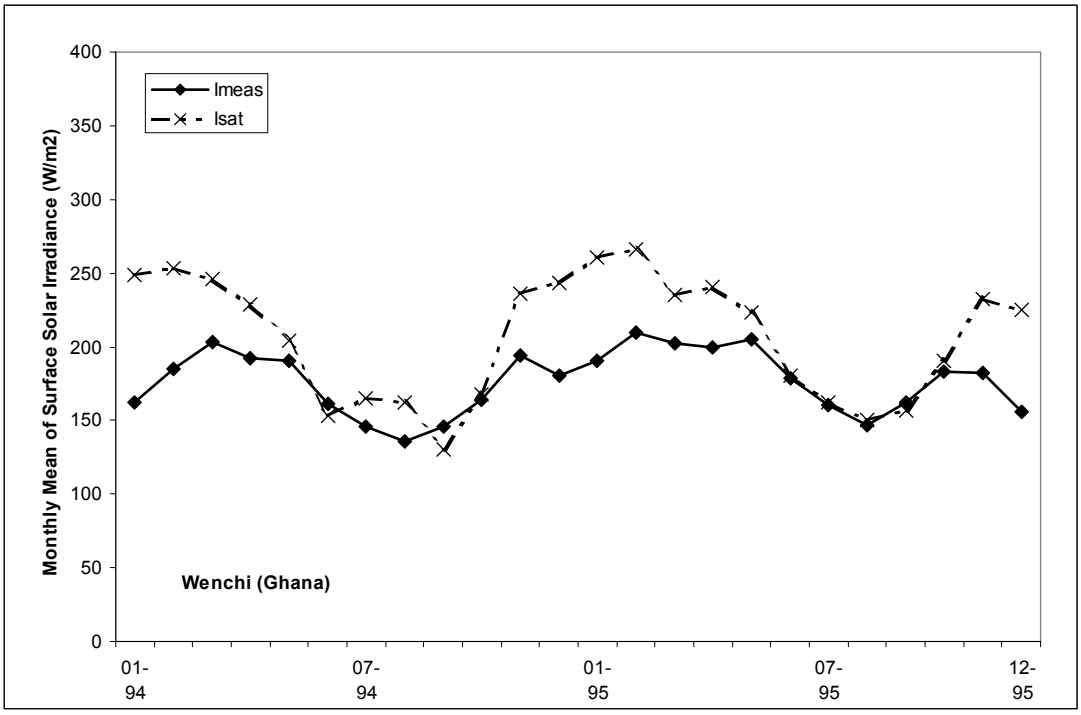
Imeas
Isat
Monthly Mean of Surface Solar Irradiance (W/m2)
400
350
300
250
200
150
100
50
0
Wenchi (Ghana)
01-94
07-94
01-95
07-95
12-95

Figure 4.

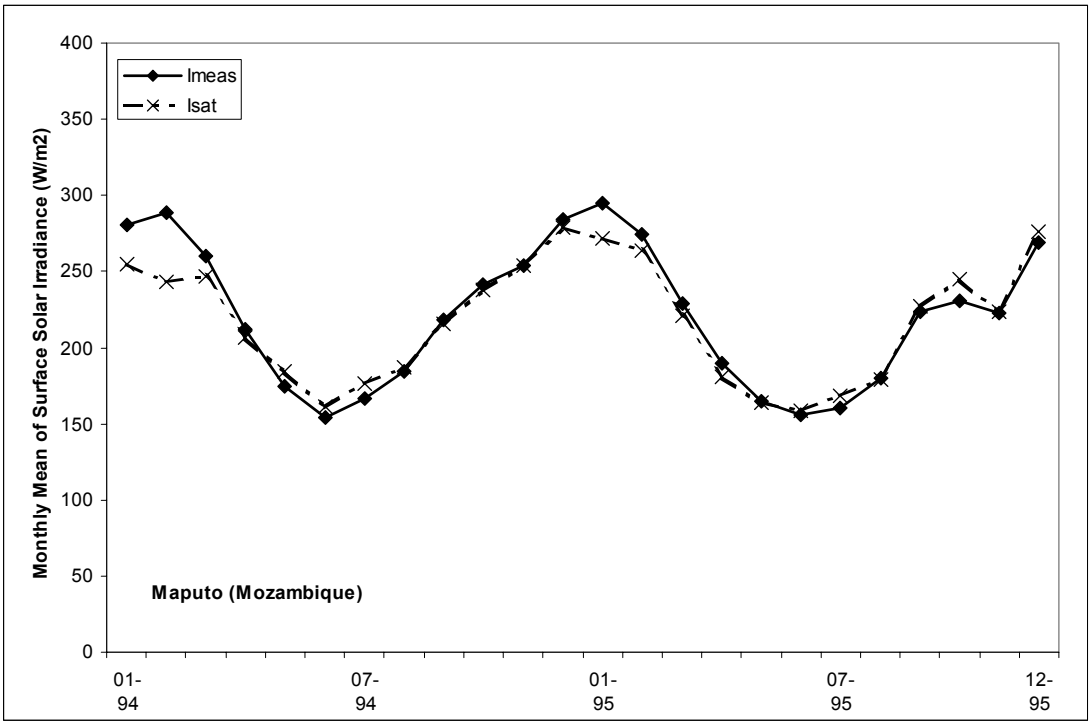
Imeas
Isat
Monthly Mean of Surface Solar Irradiance (W/m2)
400
350
300
250
200
150
100
50
0
Maputo (Mozambique)
01-94
07-94
01-95
07-95
12-95

Figure 5.

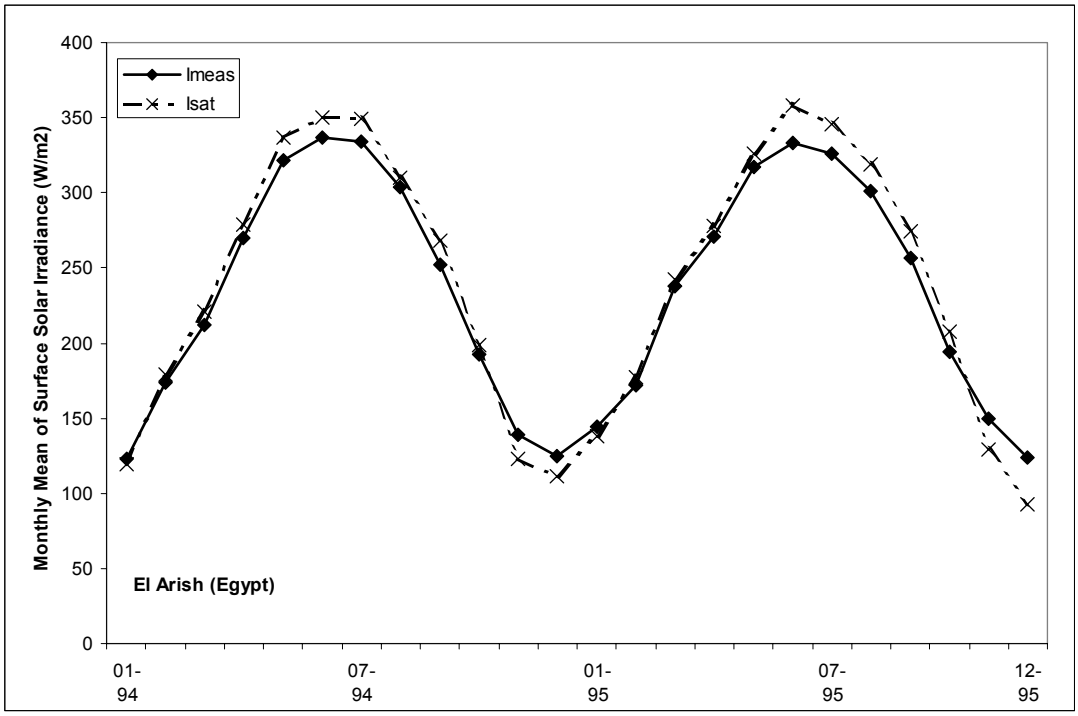
Imeas
Isat
Monthly Mean of Surface Solar Irradiance (W/m2)
El Arish (Egypt)
400
350
300
250
200
150
100
50
0
01-94
07-94
01-95
07-95
12-95

Figure 6.

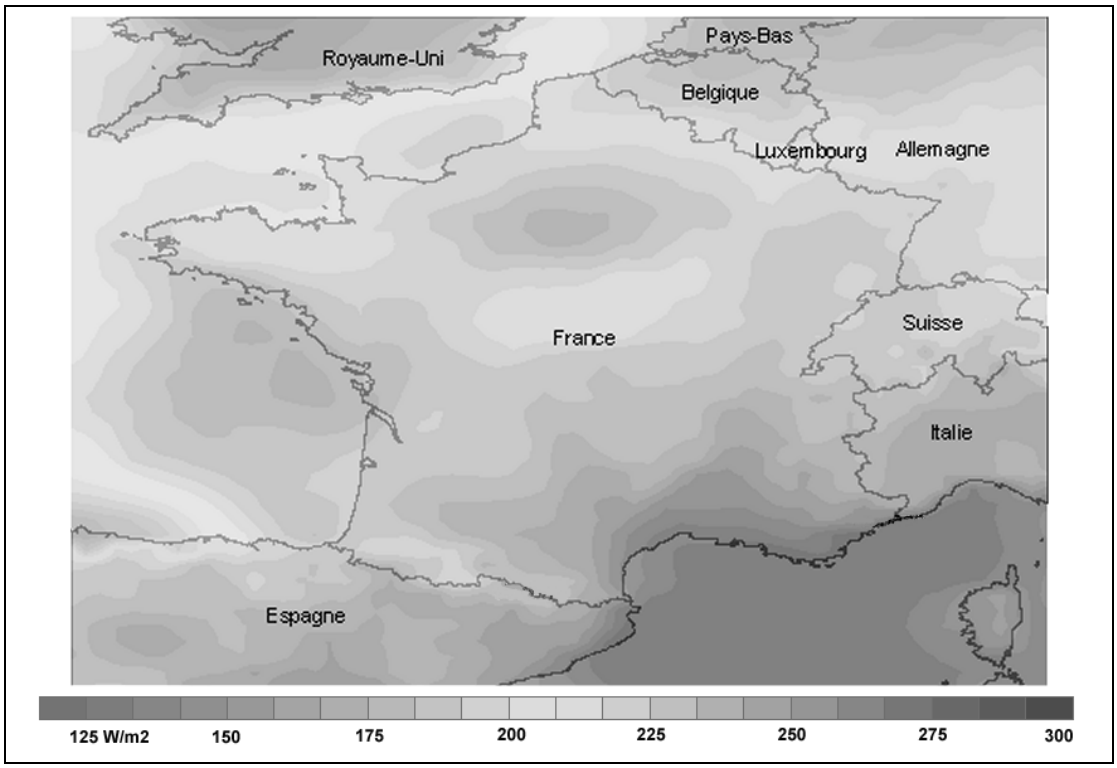
Royaume-Uni
Pays-Bas
Belgique
Luxembourg
Allemagne
France
Suisse
Italie
Espagne
125 W/m2
150
175
200
225
250
275
300

Figure 7.